

Supporting Information

Engineering Surface Structure and Defect Chemistry of Nanoscale Cubic Co₃O₄ Crystallites for Enhanced Lithium and Sodium Storage

Yanguo Liu, ^{†‡#,} Haicheng Wan, ^{†,#} Hongzhi Zhang, [†] Jiayuan Chen, [†] Fang Fang, [§] Nan Jiang, [†]
Wanxing Zhang, [†] Fangwang Zhou, [%] Hamidreza Arandiyan, ^{□,*} Yuan Wang, [¶] Guanyu Liu,[¶]
Zhiyuan Wang, ^{†‡} Shaohua Luo, ^{†‡} Xiaobo Chen, ^{%,*} Hongyu Sun ^{†,*}*

[†] School of Resources and Materials, Northeastern University at Qinhuangdao, Qinhuangdao 066004, PR China

[‡] Key Laboratory of Dielectric and Electrolyte Functional Material Hebei Province, Qinhuangdao 066004, PR China

[§] National New Energy Vehicle Technology Innovation Center, Beijing 100176, PR China

[%] Siyuan Laboratory, Guangzhou Key Laboratory of Vacuum Coating Technologies and New Energy Materials, Department of Physics, Jinan University, Guangzhou 510632, PR China

[□] Laboratory of Advanced Catalysis for Sustainability, School of Chemistry, The University of Sydney, Sydney 2006, Australia

[¶] School of Chemistry, Faculty of Science, The University of New South Wales, Sydney, New South Wales 2052, Australia

[¶] Commonwealth Scientific and Industrial Research Organisation (CSIRO), Black Mountain, Canberra, ACT 2601 Australia

[#] The authors contribute equally to this work.

Corresponding authors. E-mail addresses: lyg@neuq.edu.cn (Y.L.), hamid.arandiyan@sydney.edu.au (H.A.), txbchen@jnu.edu.cn (X.C.), hyltsun@gmail.com (H.S.).

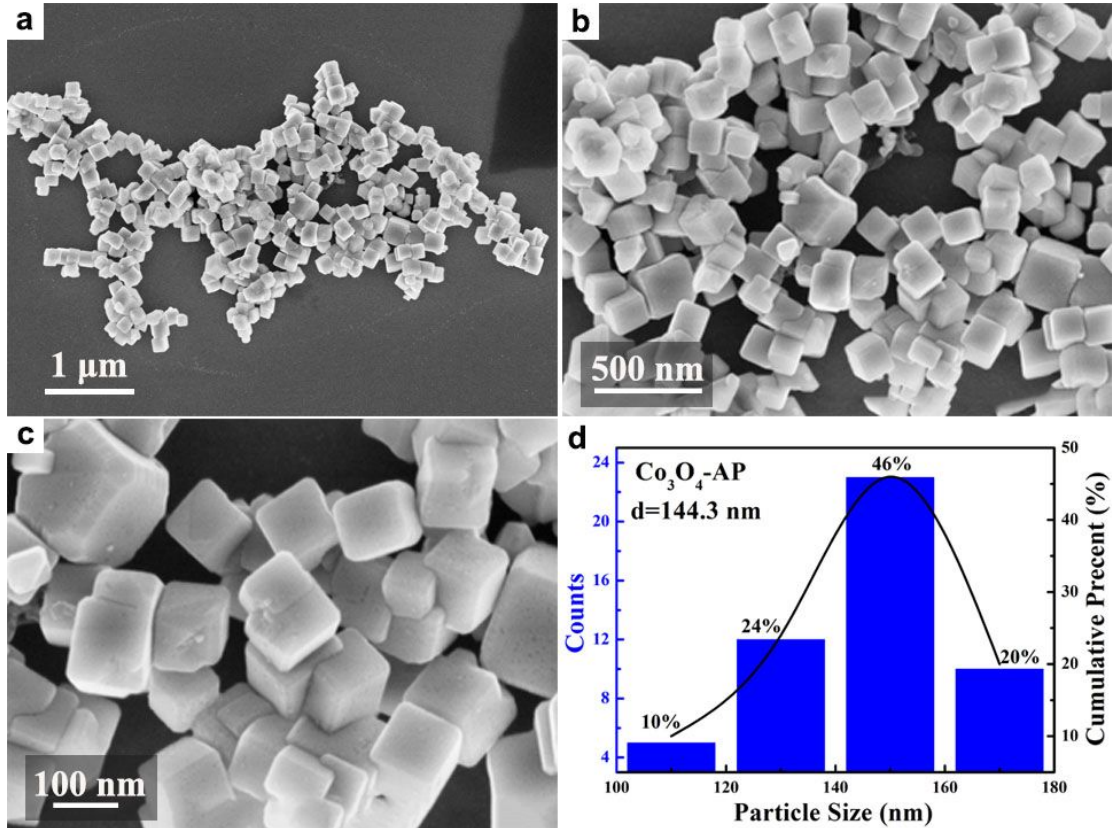


Fig. S1. (a-c) FESEM images and (d) particle size statistics of Co_3O_4 -AP sample.

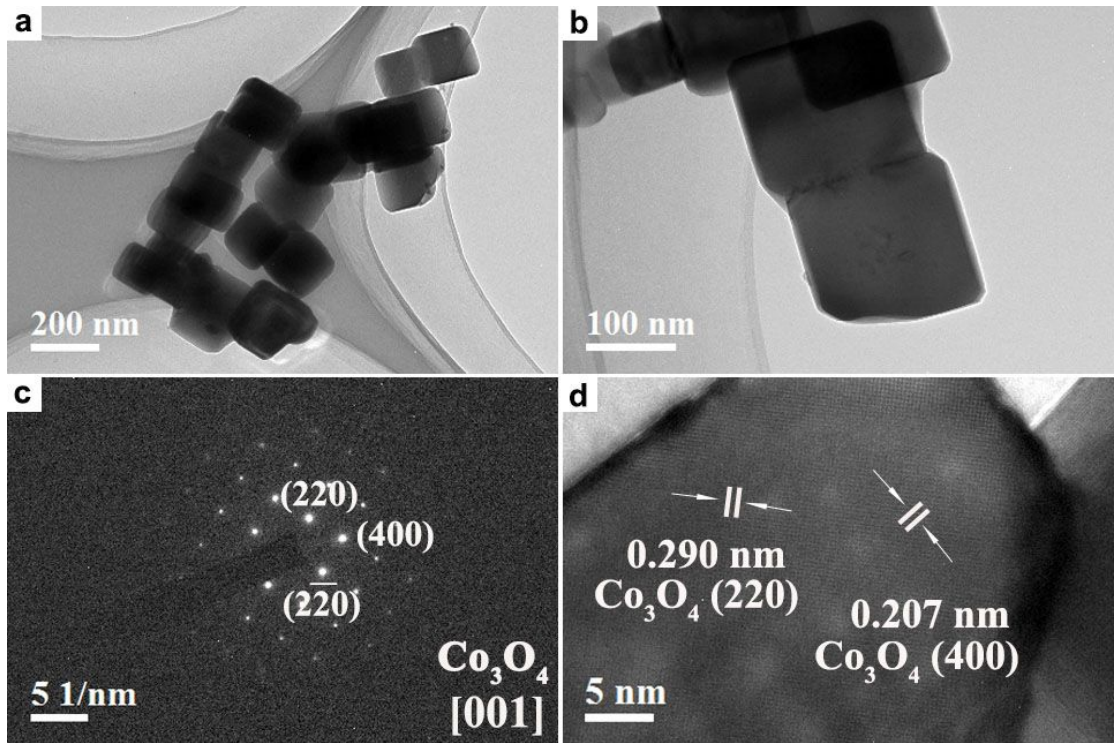


Fig. S2. (a, b) TEM images, (c) SAED pattern, and (d) HRTEM image of Co_3O_4 -AP sample.

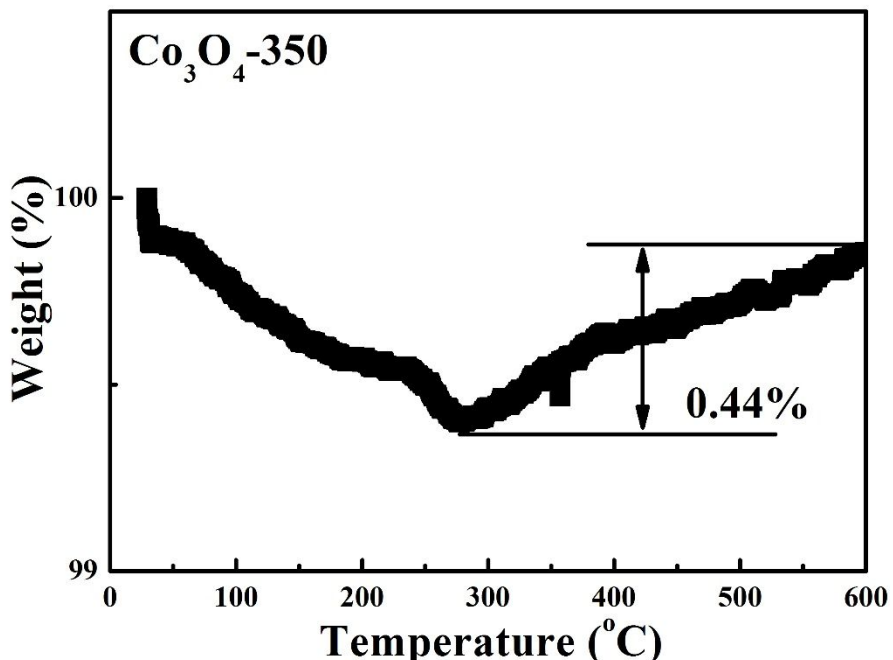


Fig. S3. Thermogravimetric curve of Co₃O₄-350 sample measured at the temperature range of 25–600 °C with a heating rate of 10 °C min⁻¹ under air atmosphere.

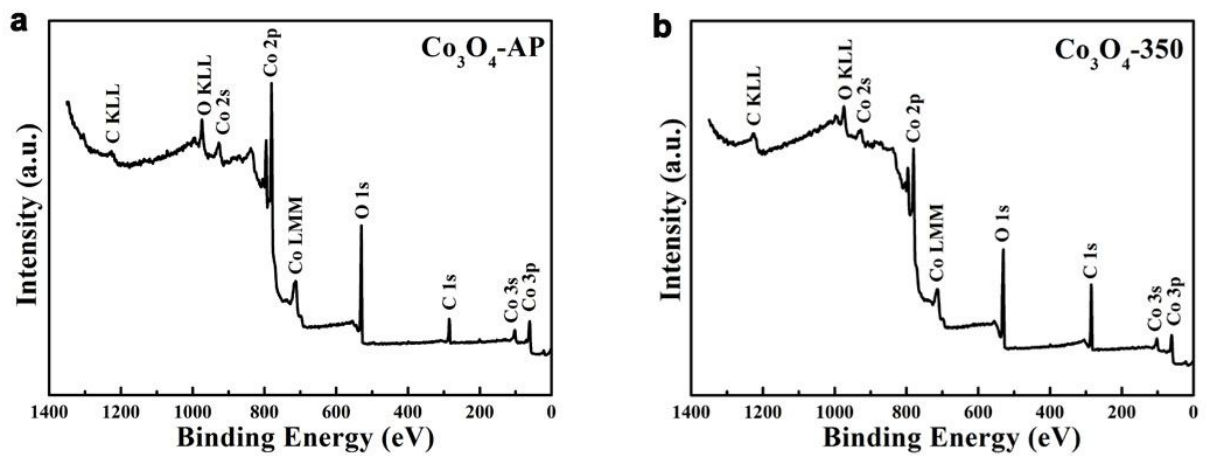


Fig. S4. XPS survey spectra of (a) Co_3O_4 -AP and (b) Co_3O_4 -350 samples.

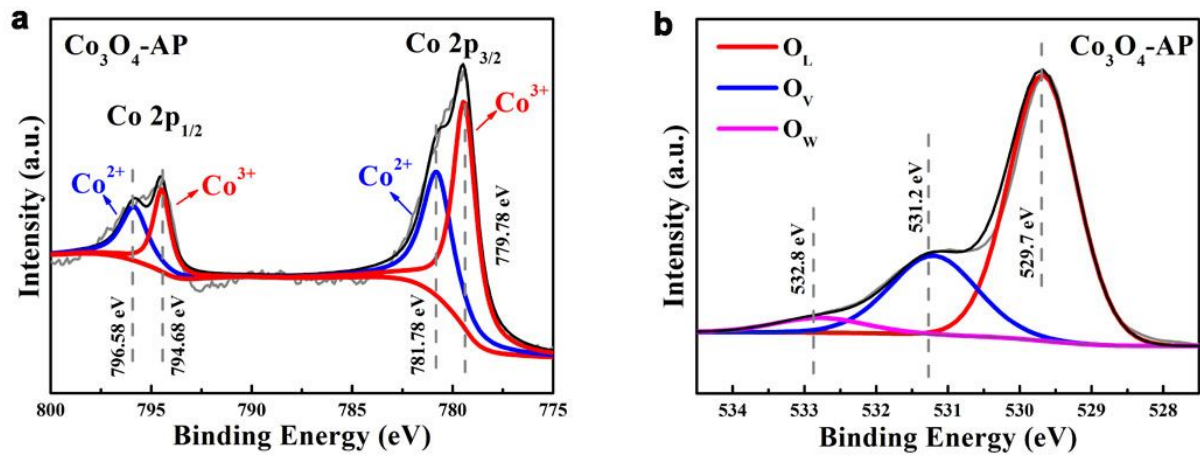


Fig. S5. High-resolution XPS spectra of Co₃O₄-AP sample: (a) Co 2p region, and (b) O 1s region.

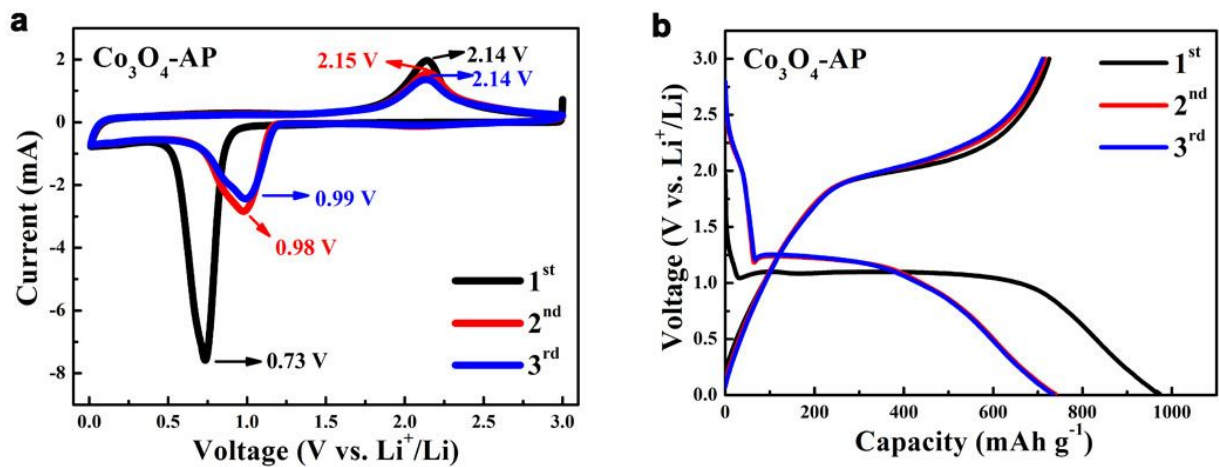


Fig. S6. (a) CV profiles of the Co₃O₄-AP electrode during the first three cycles at a scan rate of 0.5 mVs⁻¹ between 0.01 and 3 V (vs. Li⁺/Li), (b) The charge-discharge curves of Co₃O₄-AP electrode for the first three cycles between 0.01 V and 3 V vs. Li⁺/Li at a current density of 0.1 A g⁻¹.

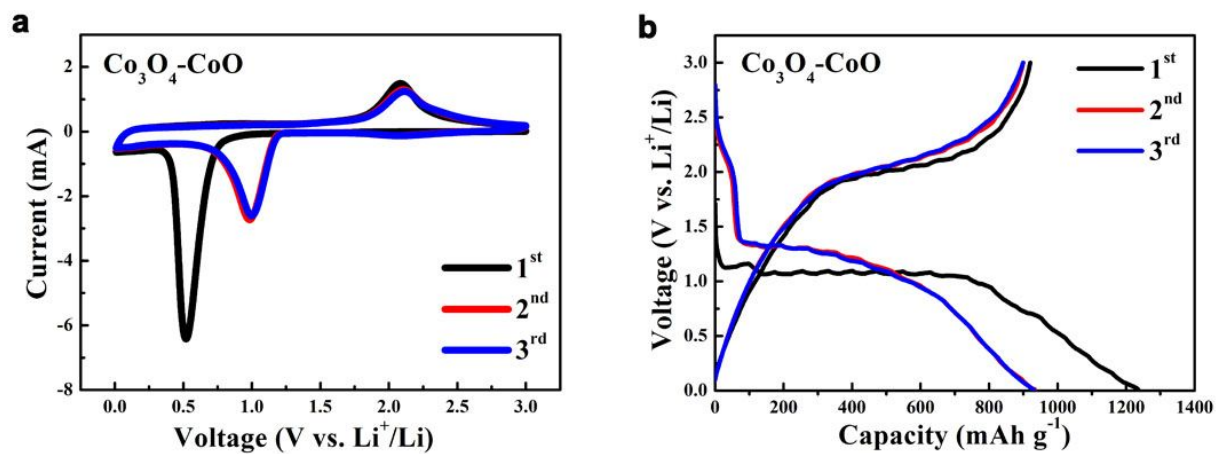


Fig. S7. (a) CV profiles of the Co_3O_4 -CoO electrode during the first three cycles at a scan rate of 0.5 mVs⁻¹ between 0.01 and 3 V (vs. Li^+/Li), (b) The charge-discharge curves of Co_3O_4 -CoO electrode for the first three cycles between 0.01 V and 3 V vs. Li^+/Li at a current density of 0.1 A g⁻¹.

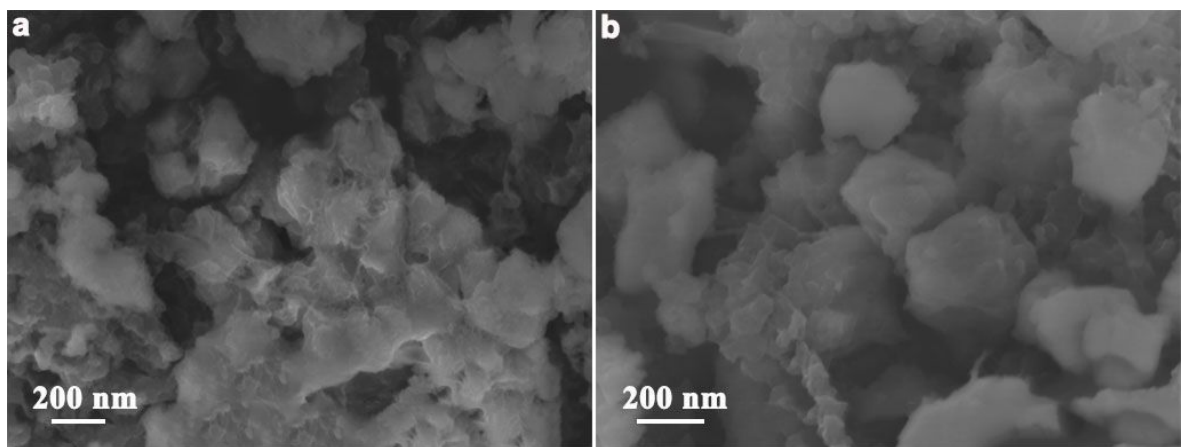


Fig. S8. FESEM images of (a) Co_3O_4 -AP and (b) Co_3O_4 -350 electrodes after cycling test.

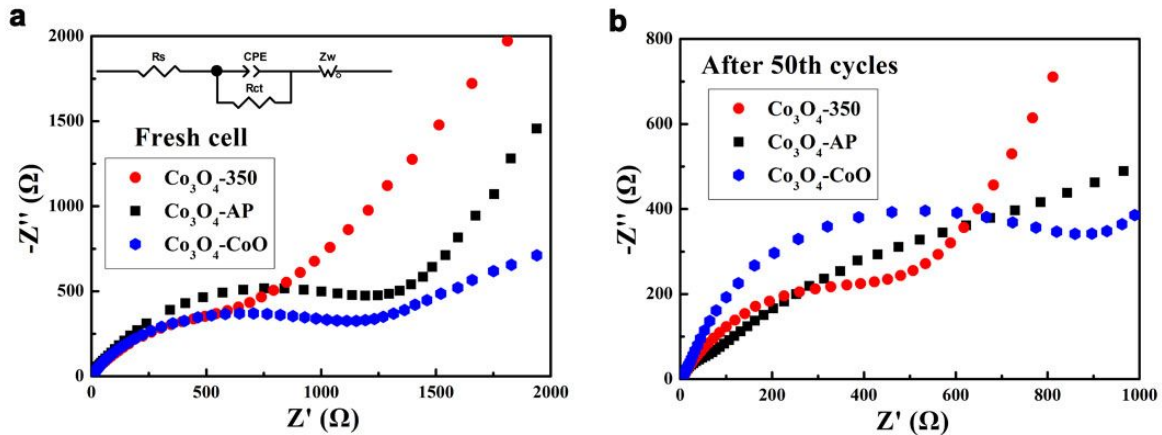


Fig. S9. Nyquist plots of $\text{Co}_3\text{O}_4\text{-AP}$ (black squares), $\text{Co}_3\text{O}_4\text{-}350$ (red circles) and $\text{Co}_3\text{O}_4\text{-CoO}$ (blue hexagons) samples used for LIBs test (a) before cycling and (b) after 50 charge-discharge cycles. The spectra were measured with an amplitude of 10 mV over the frequency range of 1 mHz and 100 kHz. The inset shows the equivalent electrical circuit used for fitting the EIS data. R_s is the electrolyte resistance, R_{ct} is the charge-transfer resistance, Z_w is the Warburg impedance, and CPE is the constant phase-angle element, respectively.

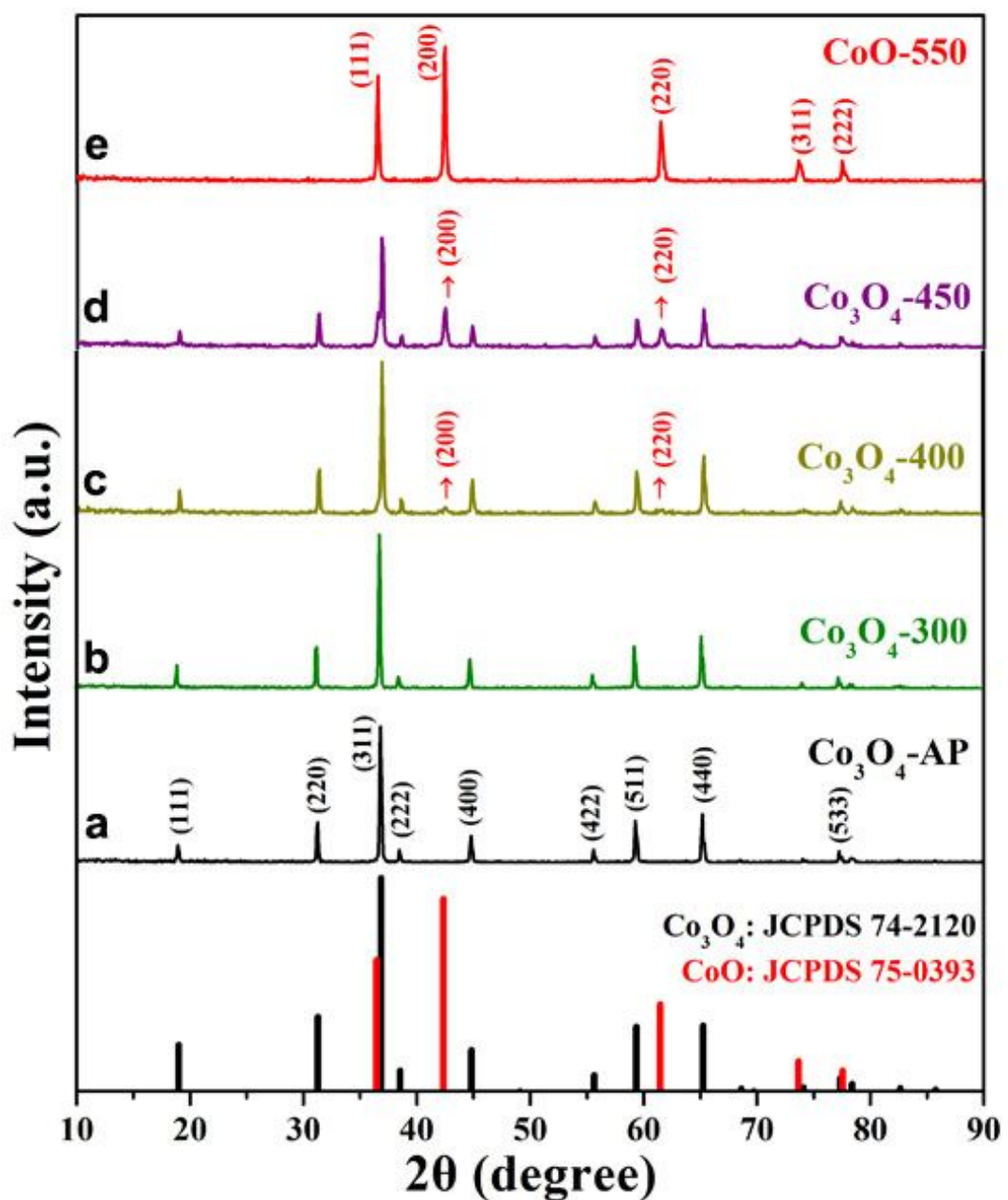


Fig. S10. XRD patterns of the Co_3O_4 samples annealed at different temperatures. The pattern of Co_3O_4 -AP is also shown for comparison.

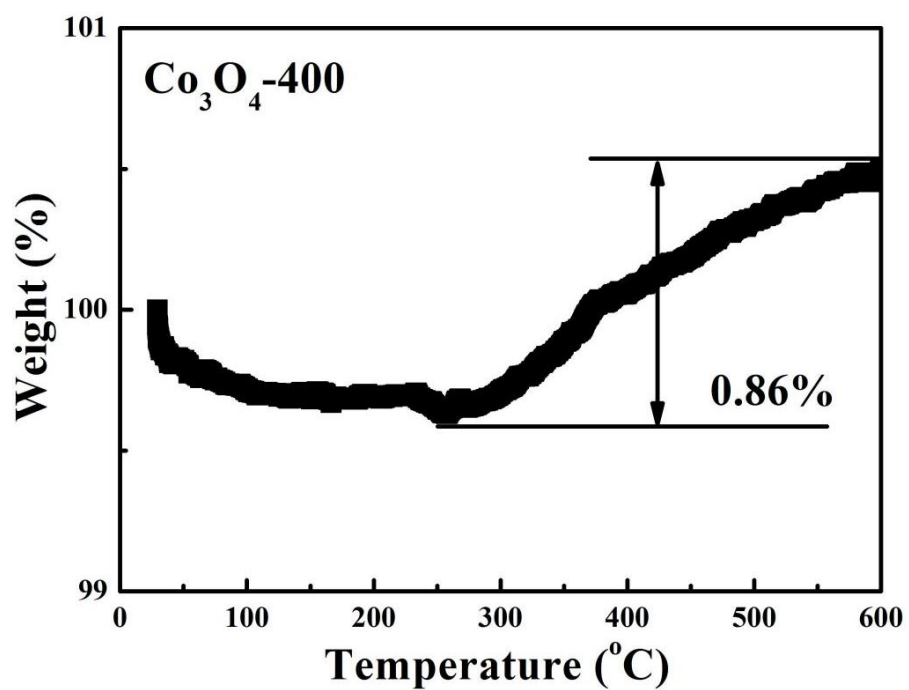


Fig. S11. Thermogravimetric curve of Co_3O_4 -400 sample measured at the temperature range of 25–600 $^{\circ}\text{C}$ with a heating rate of $10 \text{ }^{\circ}\text{C min}^{-1}$ under air atmosphere.

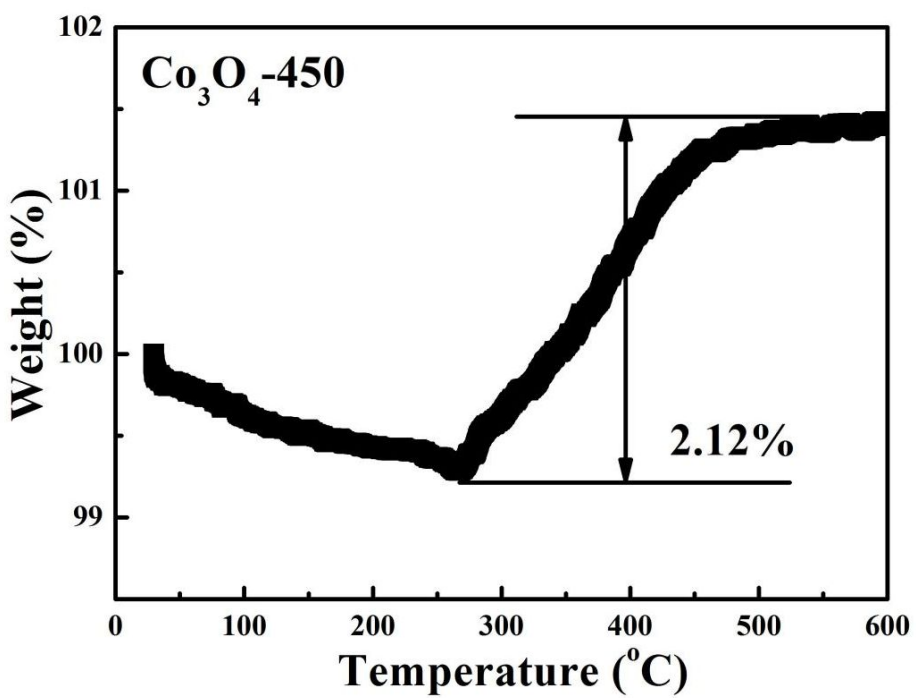


Fig. S12. Thermogravimetric curve of Co_3O_4 -450 sample measured at the temperature range of 25–600 $^{\circ}\text{C}$ with a heating rate of $10 \text{ }^{\circ}\text{C min}^{-1}$ under air atmosphere.

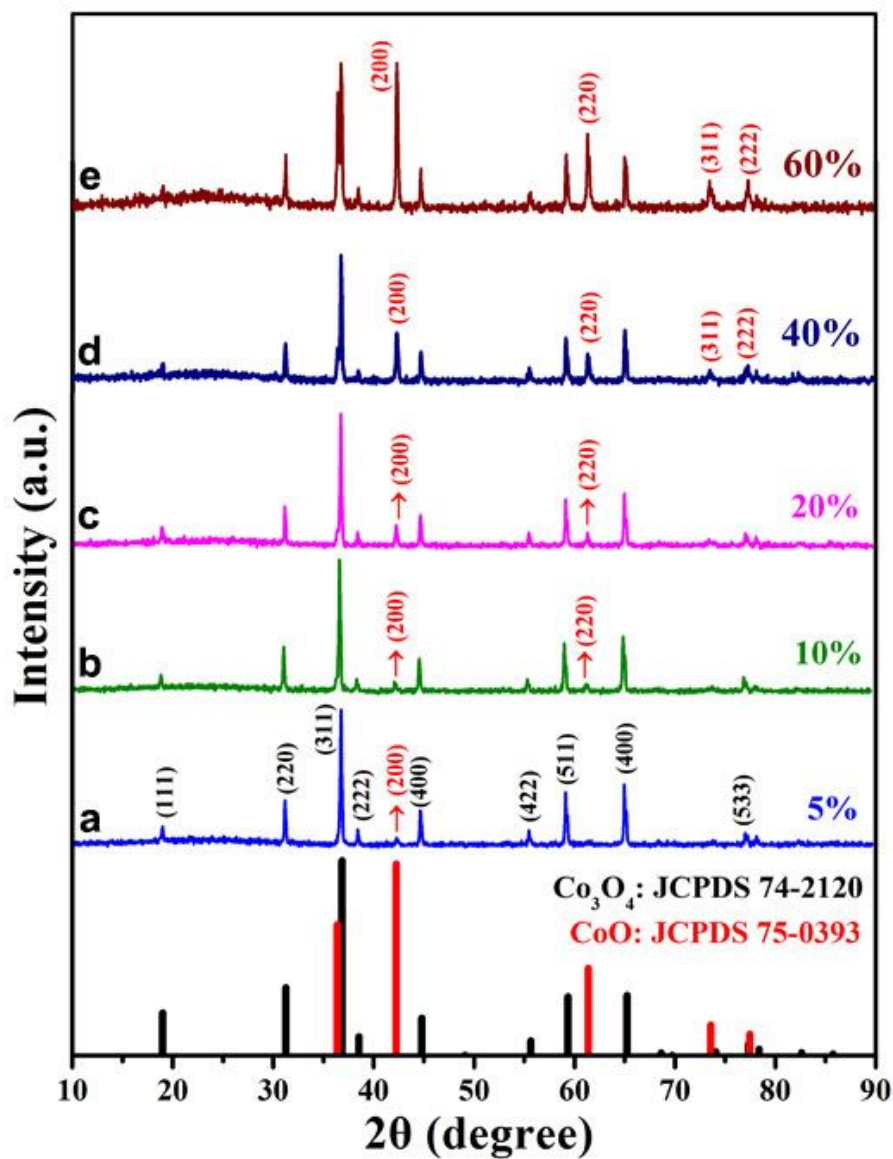


Fig. S13. XRD patterns of a series of standard samples prepared by mixing polycrystalline Co_3O_4 and CoO powders with designed composition (weight percent of $\text{CoO} = 5, 10, 20, 40, 60\%$).

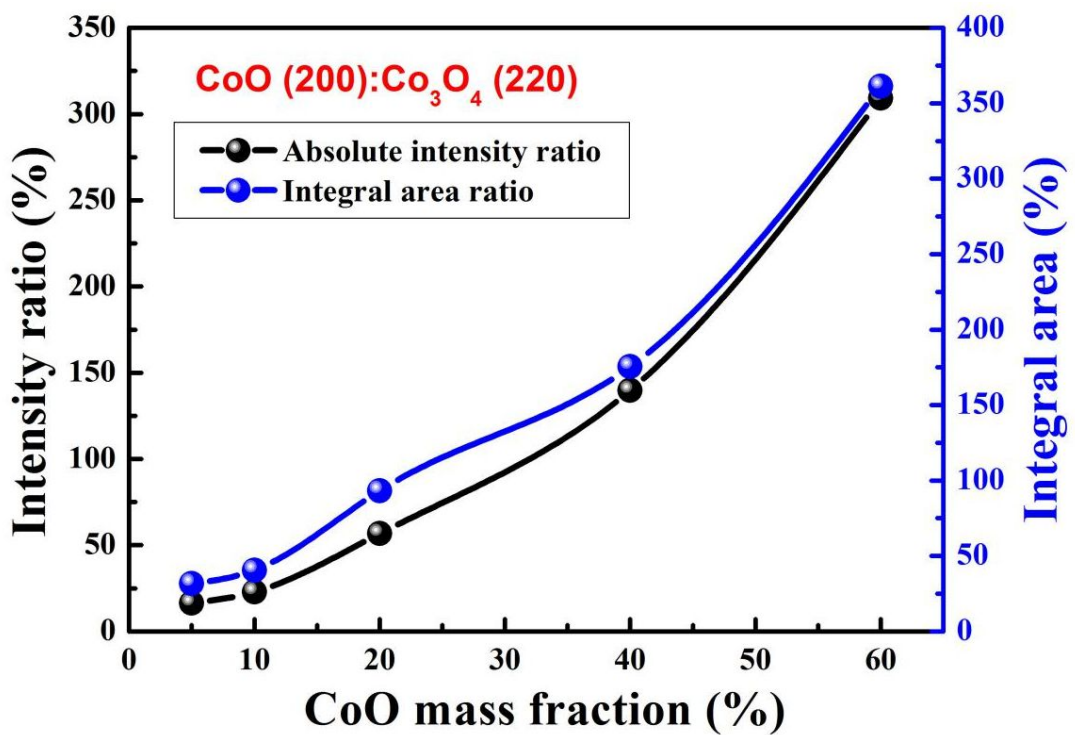


Fig. S14. The relationship between ratios of the two characteristic peaks (absolute intensity and integral area) and CoO amount in the standard samples.

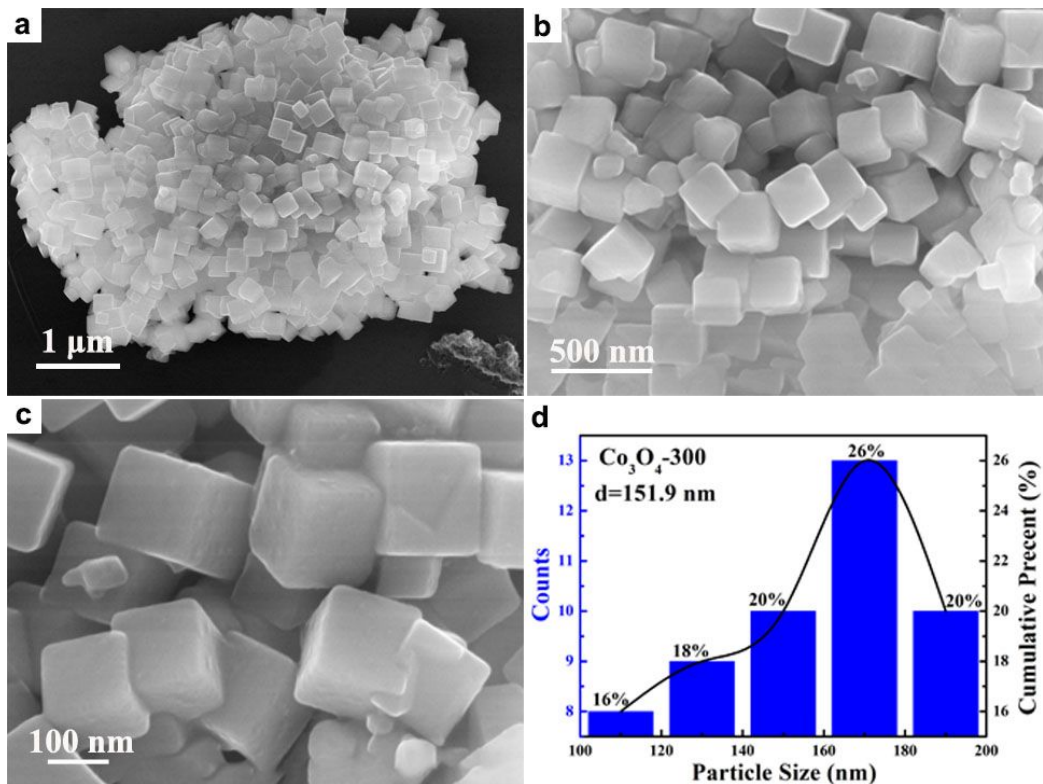


Fig. S15. (a-c) FESEM images and (d) particle size statistics of Co_3O_4 -300 sample.

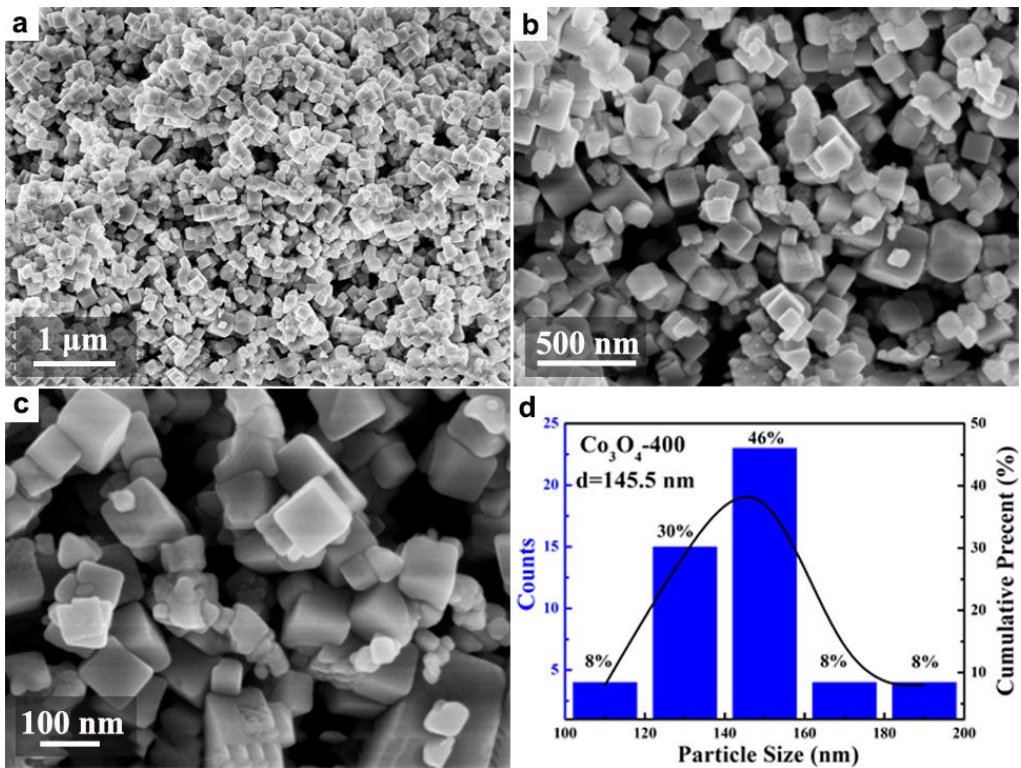


Fig. S16. (a-c) FESEM images and (d) particle size statistics of Co₃O₄-400 sample.

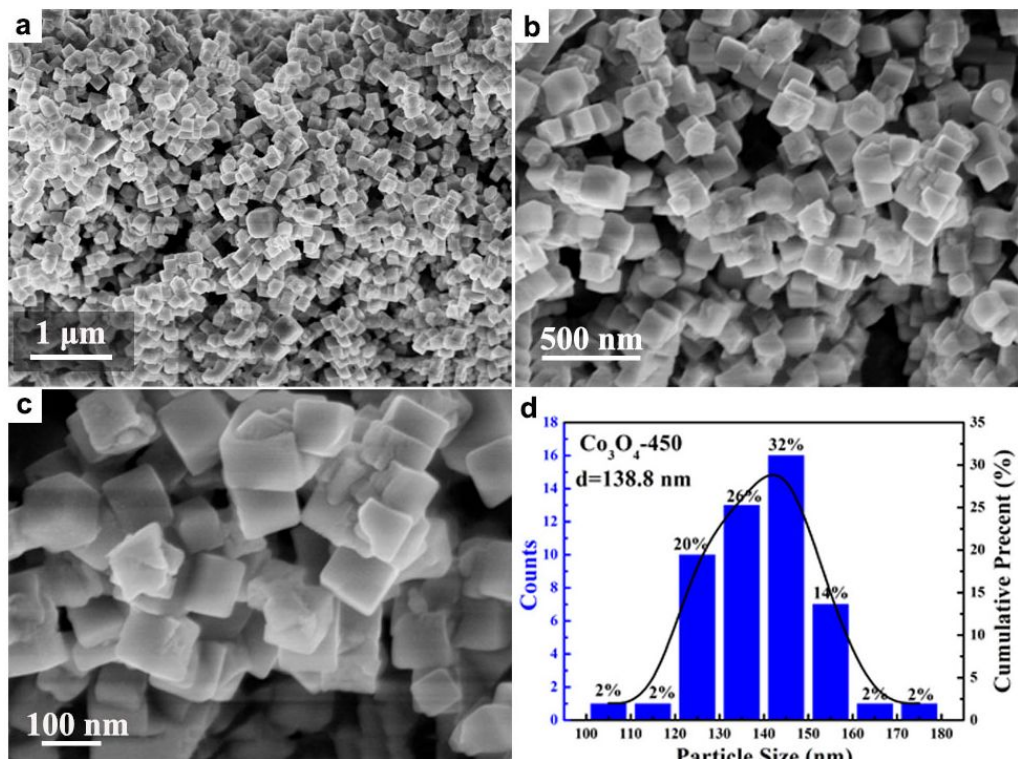


Fig. S17. (a-c) FESEM images and (d) particle size statistics of Co_3O_4 -450 sample.

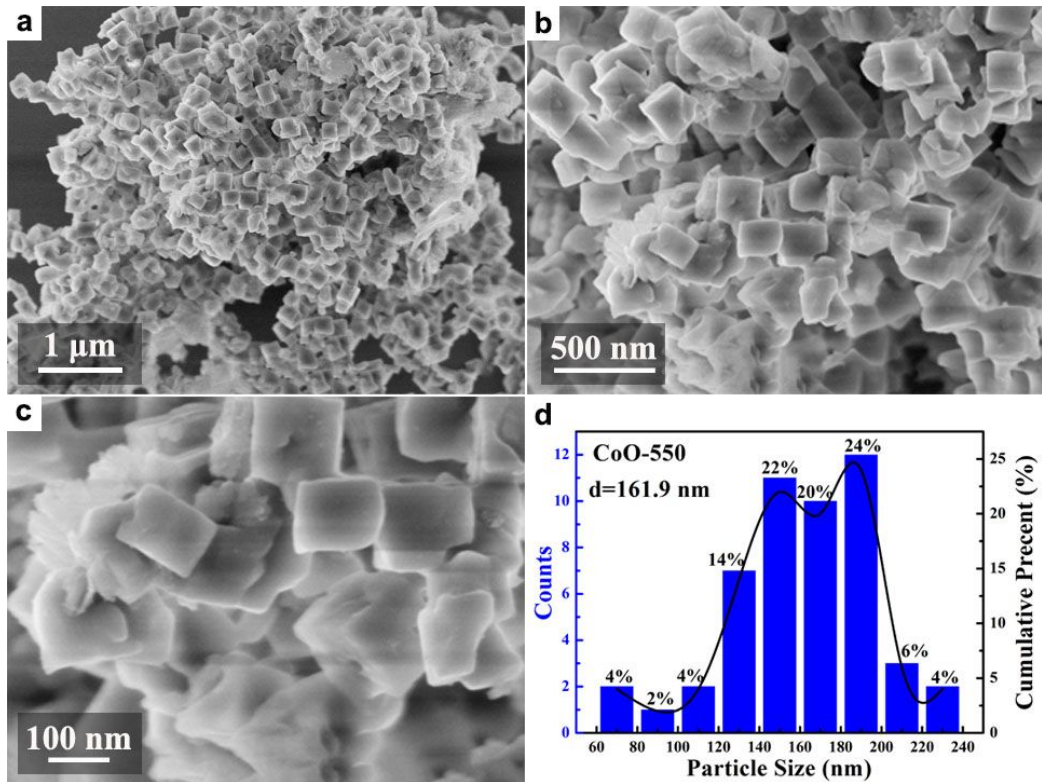


Fig. S18. (a-c) FESEM images and (d) particle size statistics of CoO-550 sample.

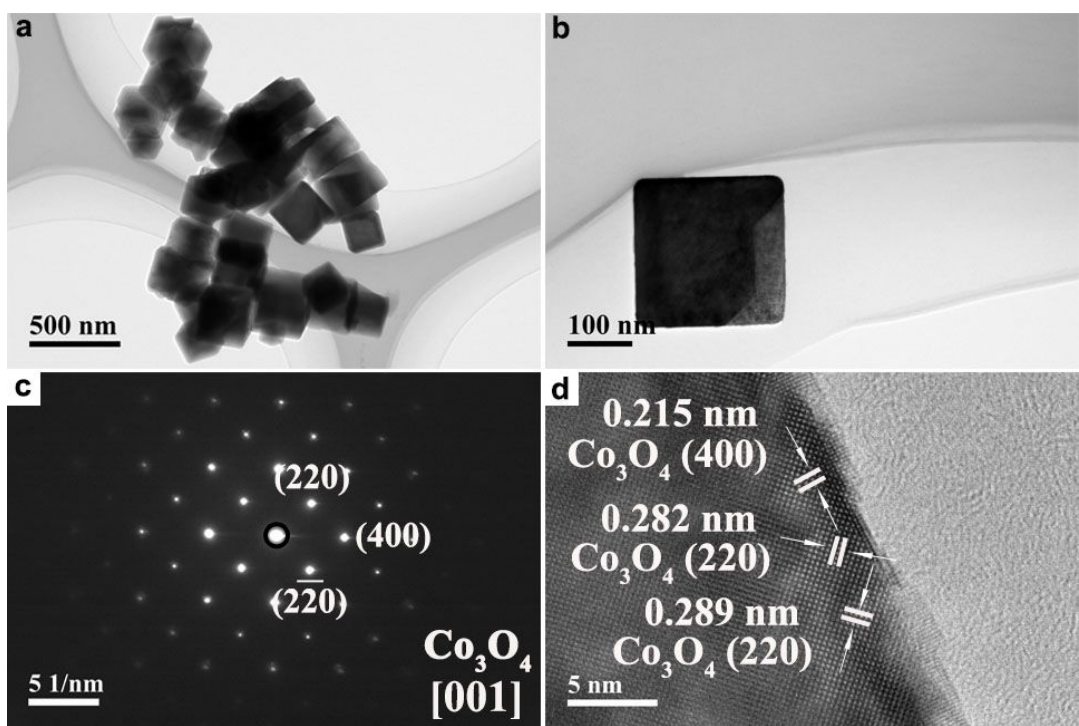


Fig. S19. (a, b) TEM images, (c) SAED pattern, and (d) HRTEM image of Co_3O_4 -300 sample.

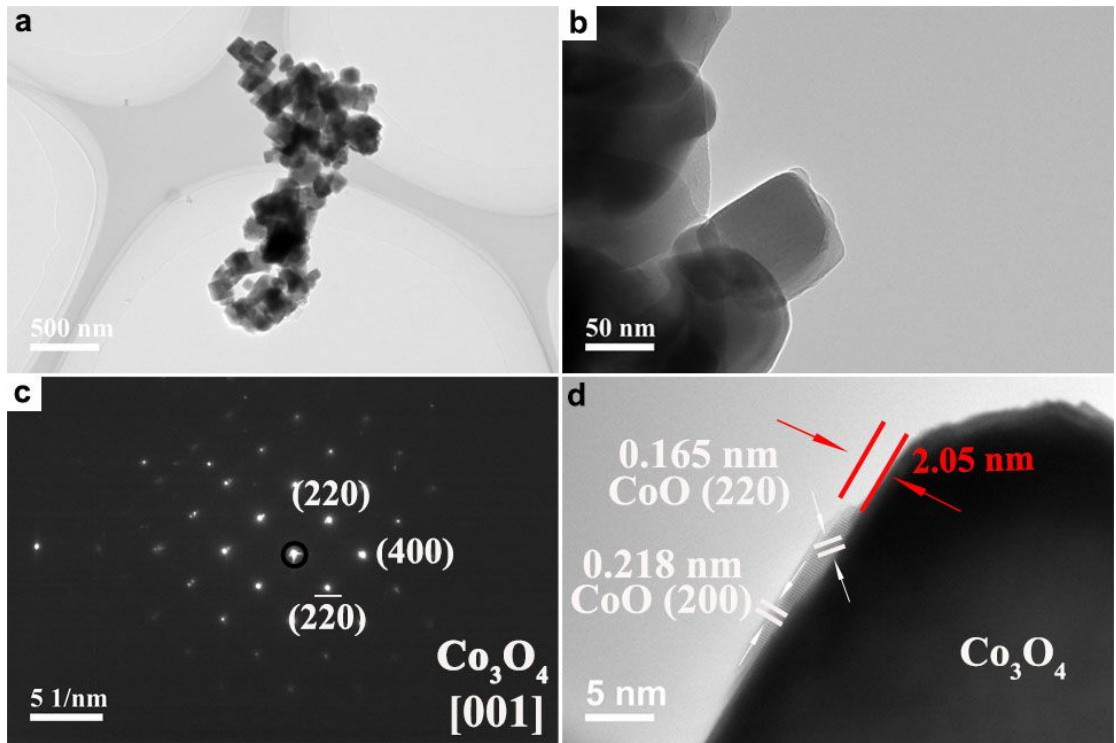


Fig. S20. (a, b) TEM images, (c) SAED pattern, and (d) HRTEM image of Co_3O_4 -400 sample.

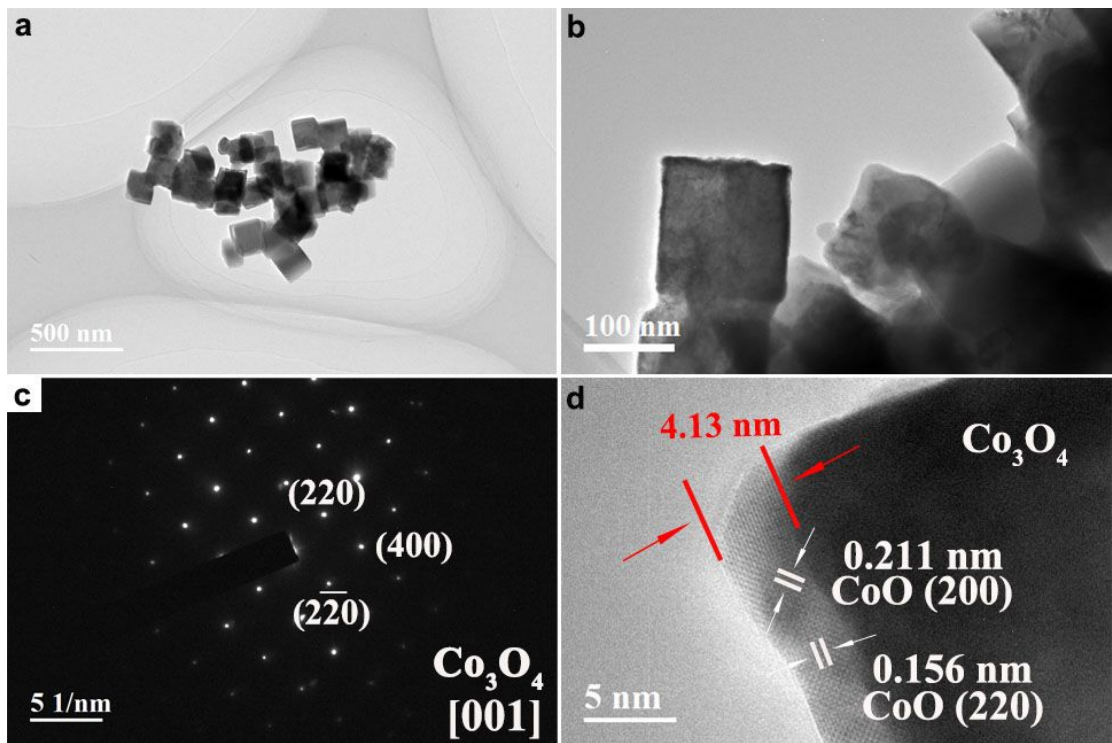


Fig. S21. (a, b) TEM images, (c) SAED pattern, and (d) HRTEM image of Co_3O_4 -450 sample.

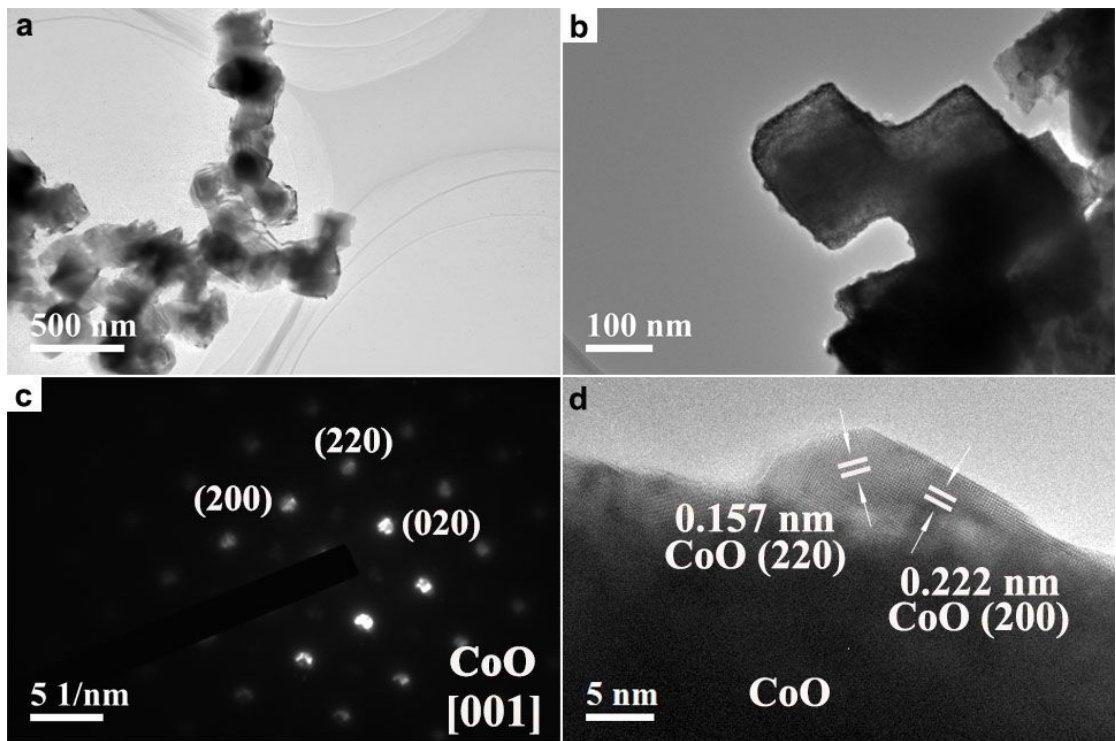


Fig. S22. (a, b) TEM images, (c) SAED pattern, and (d) HRTEM image of CoO-550 sample.

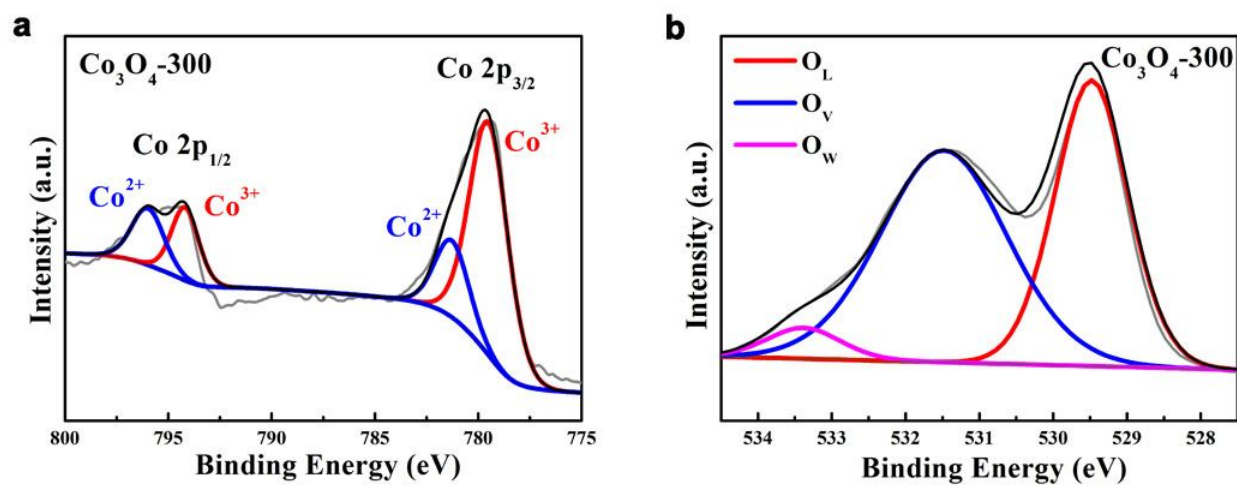


Fig. S23. High-resolution XPS spectra of Co₃O₄-300 sample: (a) Co 2p region, and (b) O 1s region.

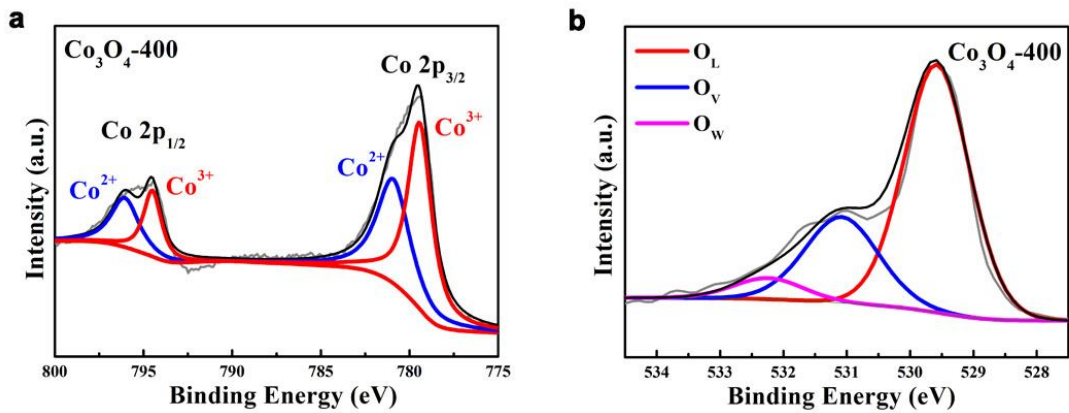


Fig. S24. High-resolution XPS spectra of Co₃O₄-400 sample: (a) Co 2p region, and (b) O 1s region.

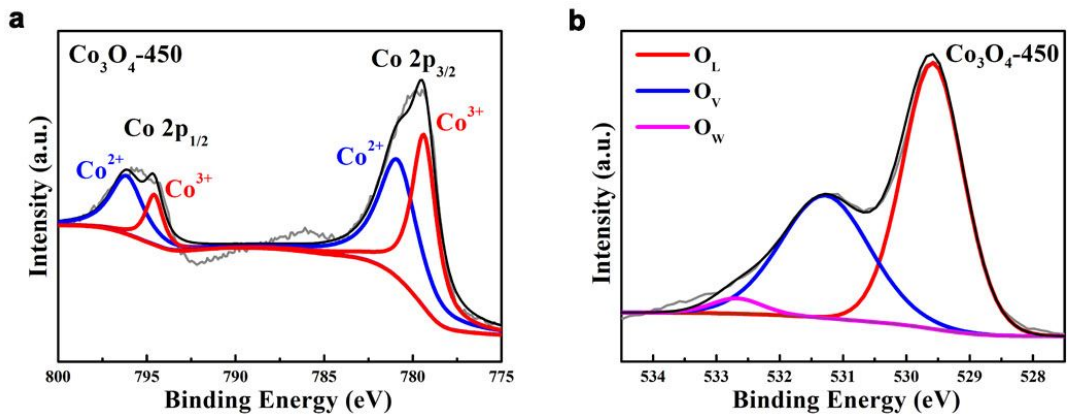


Fig. S25. High-resolution XPS spectra of Co₃O₄-450 sample: (a) Co 2p region, and (b) O 1s region.

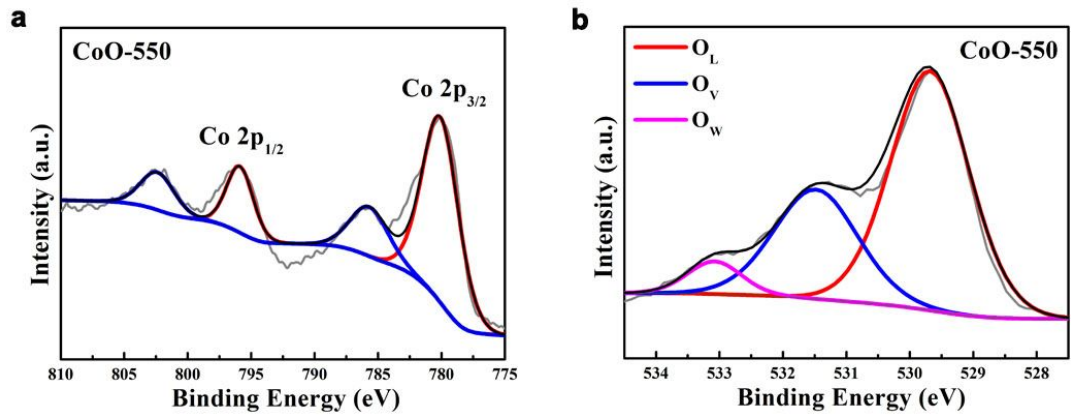


Fig. S26. High-resolution XPS spectra of CoO-550 sample: (a) Co 2p region, and (b) O 1s region.

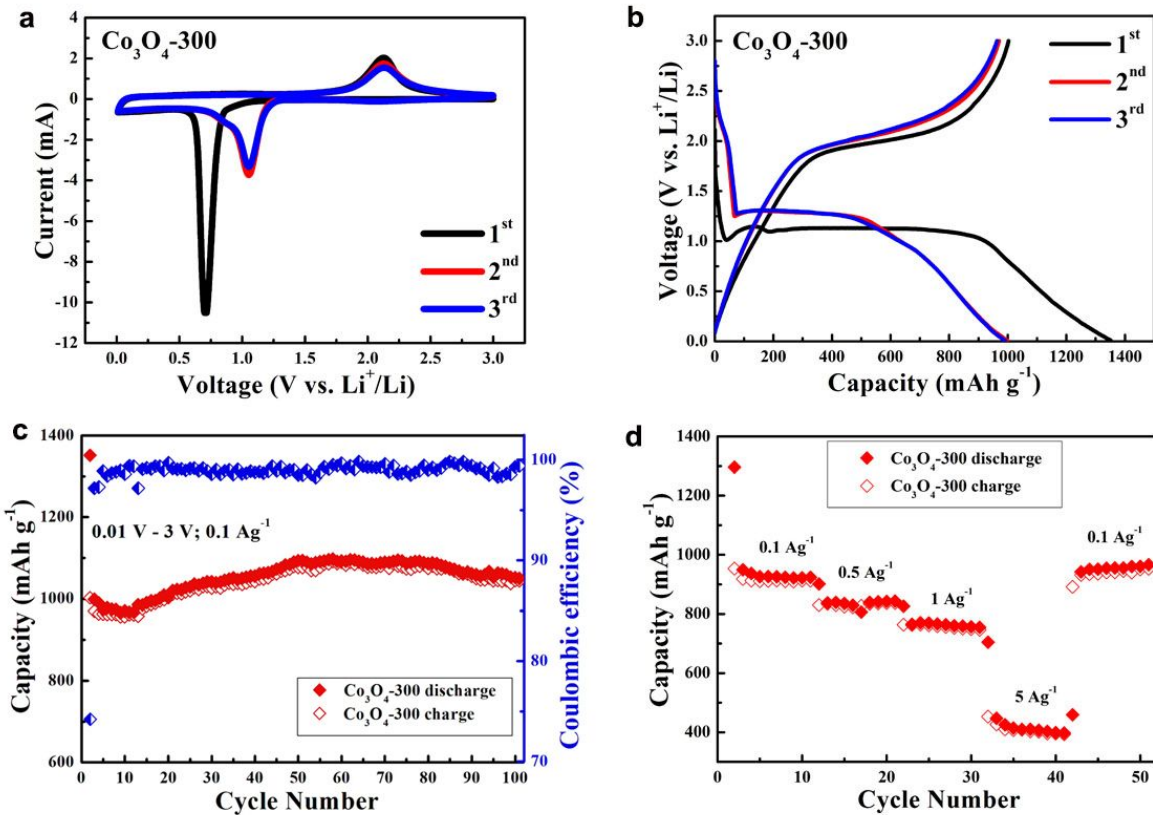


Fig. S27. Electrochemical performance of Co_3O_4 -300 sample: (a) CV profiles during the first three cycles at a scan rate of 0.5 mVs^{-1} between 0.01 and 3 V (vs. Li^+/Li), (b) The charge-discharge curves for the first three cycles between 0.01 V and 3 V vs. Li^+/Li at a current density of 0.1 A g^{-1} , (c) cycling performance and (d) rate capability.

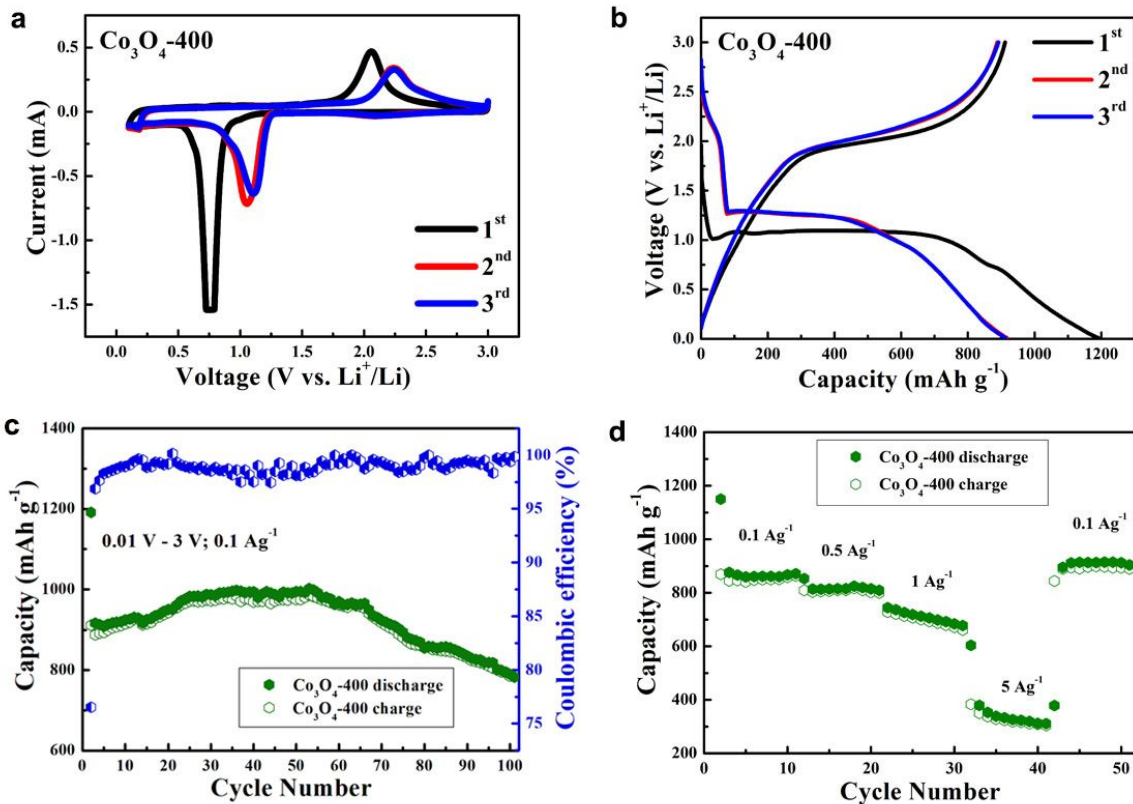


Fig. S28. Electrochemical performance of Co_3O_4 -400 sample: (a) CV profiles during the first three cycles at a scan rate of 0.5 mVs^{-1} between 0.01 V and 3 V (vs. Li^+/Li), (b) The charge-discharge curves for the first three cycles between 0.01 V and 3 V vs. Li^+/Li at a current density of 0.1 A g^{-1} , (c) cycling performance and (c) rate capability.

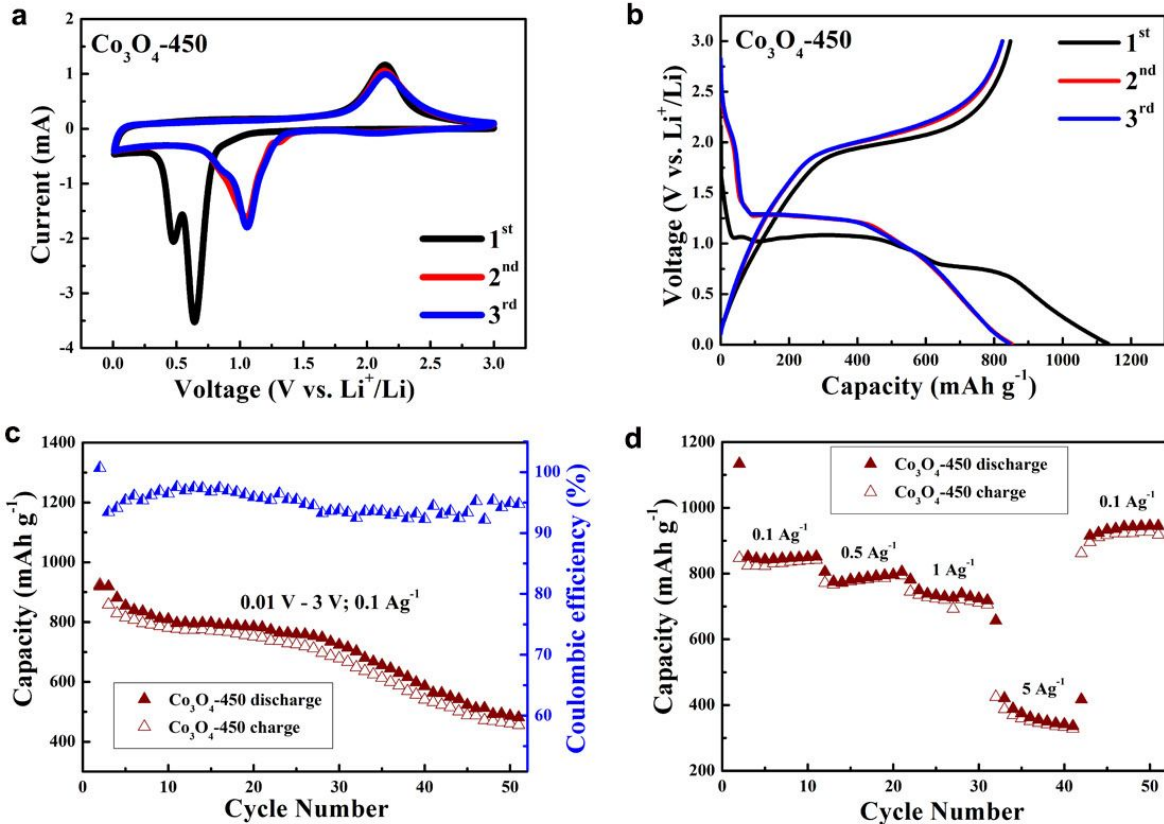


Fig. S29. Electrochemical performance of Co_3O_4 -450 sample: (a) CV profiles during the first three cycles at a scan rate of 0.5 mVs⁻¹ between 0.01 and 3 V (vs. Li⁺/Li), (b) The charge-discharge curves for the first three cycles between 0.01 V and 3 V vs. Li⁺/Li at a current density of 0.1 A g⁻¹, (c) cycling performance and (c) rate capability.

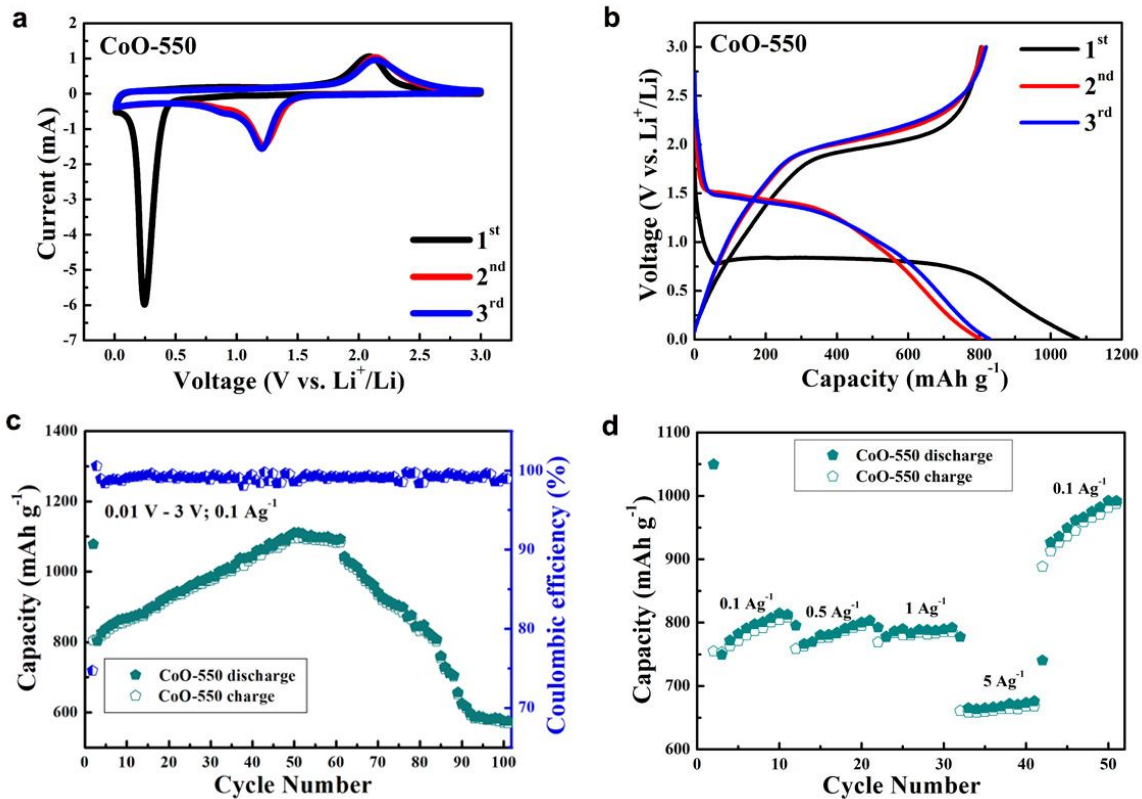


Fig. S30. Electrochemical performance of CoO-550 sample: (a) CV profiles during the first three cycles at a scan rate of 0.5 mVs⁻¹ between 0.01 and 3 V (vs. Li⁺/Li), (b) The charge-discharge curves for the first three cycles between 0.01 V and 3 V vs. Li⁺/Li at a current density of 0.1 A g⁻¹, (c) cycling performance and (c) rate capability.

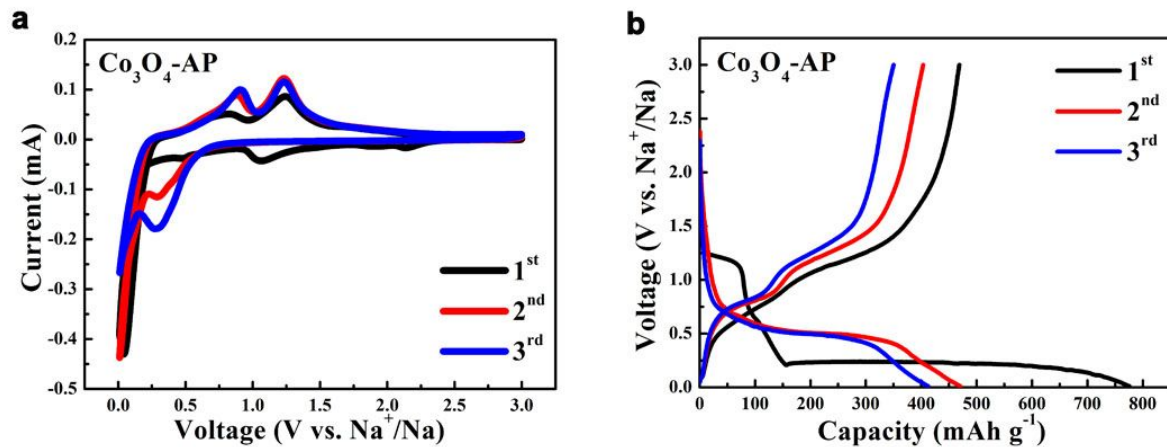


Fig. S31. (a) CV profiles of the Co_3O_4 -AP electrode during the first three cycles at a scan rate of 0.5 mVs⁻¹ between 0.01 and 3 V (vs. Na^+/Na), (b) The charge-discharge curves of Co_3O_4 -AP electrode for the first three cycles between 0.01 V and 3 V vs. Na^+/Na at a current density of 0.025 A g⁻¹.

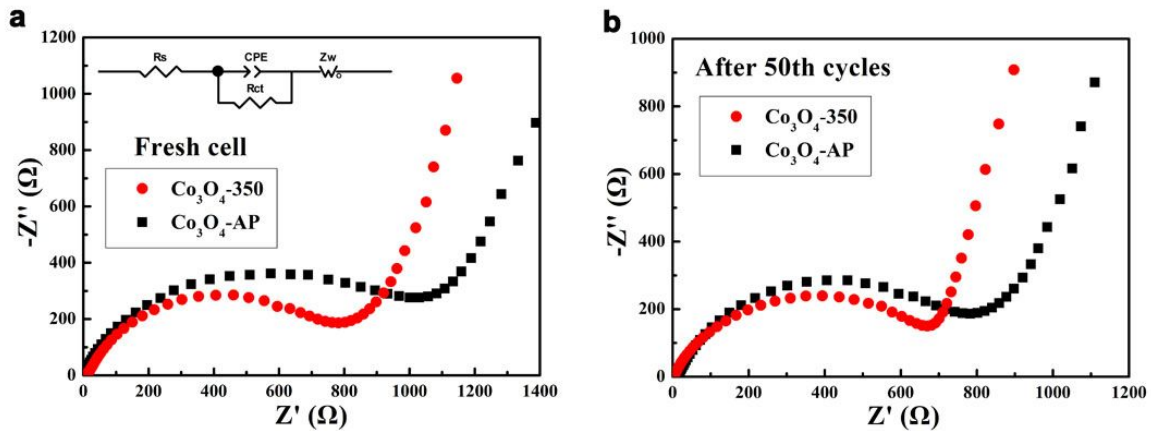


Fig. S32. Nyquist plots of Co_3O_4 -AP (black squares) and Co_3O_4 -350 (red circles) samples used for SIBs

test (a) before cycling and (b) after 50 charge-discharge cycles. The spectra were measured with an amplitude of 10 mV over the frequency range of 1 mHz and 100 kHz. The inset shows the equivalent electrical circuit used for fitting the EIS data. R_s is the electrolyte resistance, R_{ct} is the charge-transfer resistance, Z_w is the Warburg impedance, and CPE is the constant phase-angle element, respectively.

Table S1. Kinetic parameters of Co_3O_4 -350, Co_3O_4 -AP, and Co_3O_4 -CoO cells.

Cells	R_s/Ω	CPE/F	R_{ct}/Ω	Z_w/Ω
Co_3O_4 -350 before cycling	1.82	2.87×10^{-5}	1048	3019
Co_3O_4 -AP before cycling	9.61	8.36×10^{-5}	2264	17074
Co_3O_4 -CoO before cycling	3.89	1.87×10^{-5}	1235	2709
Co_3O_4 -350 after cycling	0.70	1.14×10^{-5}	805.9	2666
Co_3O_4 -AP after cycling	0.86	1.99×10^{-5}	1281	4651
Co_3O_4 -CoO after cycling	2.55	1.53×10^{-5}	1140	2680

Table S2. CoO layer thickness in the composite samples (Co_3O_4 -350, Co_3O_4 -400, and Co_3O_4 -450). The values in bracket are the weight percent of CoO calculated by the according methods. (*, see Fig. S14)

	Co_3O_4 -350	Co_3O_4 -400	Co_3O_4 -450
TGA	1.62 nm (6.6%)	3.09 nm (12.9%)	7.91 nm (31.8%)
XRD (absolute intensity ratio) *	0.73 nm (3%)	0.97 nm (4.2%)	7.34 nm (29.8%)
XRD (integral area ratio) *	0.48 nm (2%)	1.38 nm (5.9%)	9.36 nm (36.7%)
HRTEM	1.13 nm	2.05 nm	4.13 nm

Table S3. Performance comparison of some LIB anodes based on typical Co₃O₄ structures.

materials	reversible capacity(cycles)	rate capability	voltage range	Ref
	/mA h g ⁻¹	/mA h g ⁻¹	/V, vs. Li ⁺ /Li	
triple shelled Co ₃ O ₄ hollow microspheres	1615.8 (30) @0.05 A g ⁻¹	1117.3 @2 A g ⁻¹	0.05 – 3.0	1
micron sized Co ₃ O ₄ hollow powders	702 (300) @1 A g ⁻¹	581 @10 A g ⁻¹	0.001-3.0	2
Co ₃ O ₄ nanotubes	380 (80) @0.05 A g ⁻¹	—	0.01-3.0	3
porous Co ₃ O ₄ hollow dodecahedra	780 (100) @0.1 A g ⁻¹	610 @8.9 A g ⁻¹	0.01 – 3.0	4
mesoporous and single-crystal Co ₃ O ₄ arrays	788.7 (25) @1.34 A g ⁻¹	320 @26.7 A g ⁻¹	—	5
Co ₃ O ₄ mesoporous nanostructures	889 (80) @0.2 A g ⁻¹	804 @1 A g ⁻¹	0.01-3.0	6
bacteria directed porous Co ₃ O ₄	903 (20) @0.18 A g ⁻¹	—	0.01 – 3.0	7
mesoporous quasi-single-crystalline Co ₃ O ₄ nanobelts	1400 (20) @0.05 A g ⁻¹	1333.4 @0.9 A g ⁻¹	0 – 3.0	8
Co ₃ O ₄ octahedra	714 (50) @1 A g ⁻¹	700 @2 A g ⁻¹	0.01 – 3.0	9
Co ₃ O ₄ nanocubes	650 (400) @0.5 A g ⁻¹	610 @2 A g ⁻¹	0.01-3.0	10
mesoporous Co ₃ O ₄ nanoflowers	980 (30) @0.05 A g ⁻¹	875 @0.5 A g ⁻¹	0.01 – 3.0	11
Micro-/Nanostructured Co ₃ O ₄	980 (60) @0.1 A g ⁻¹	130 @10 A g ⁻¹	0.01-3.0	12
Co ₃ O ₄ nanocages with highly exposed {110} facets	864 (50) @0.18 A g ⁻¹	700 @1.78 A g ⁻¹ 216 @4.45 A g ⁻¹	—	13
SiO ₂ -doped Co ₃ O ₄ hollow nanospheres	971 (150) @2 A g ⁻¹	853 @3 A g ⁻¹	0.001-3.0	14
peapod-like Co ₃ O ₄ @CNT arrays	862 (100) @0.1A g ⁻¹	408 @5 A g ⁻¹	0 – 3.0	15
3D Co ₃ O ₄ and CoO@C wall arrays	804 (60) @0.5 A g ⁻¹	420 @1 A g ⁻¹	0.01-3.0	16
Co ₃ O ₄ nanoparticles confined into single-walled carbon nanotube matrix	530 (200) @1 A g ⁻¹	425 @5 A g ⁻¹	0.01-3.0	17
MWCNTs/Co ₃ O ₄ derived from MOF	813 (100) @0.1A g ⁻¹	514 @1 A g ⁻¹	0.01 – 3.0	18
atomically thin Co ₃ O ₄ nanosheets/graphene composite	851.5 (2000) @2 A g ⁻¹	509.3 @5 A g ⁻¹	0.01 – 3.0	19
Co ₃ O ₄ @carbon	1050 (50) @0.89 A g ⁻¹	380 @8.9 A g ⁻¹	0.01 – 3.0	20
Carbon-doped Co ₃ O ₄ nanocrystals	950 (300) @0.5 A g ⁻¹	853 @10 A g ⁻¹	0.01-3.0	21
Co ₃ O ₄ /C composite	928 (50) @0.2 A g ⁻¹	470 @3.2 A g ⁻¹	0.01-3.0	22
Co ₃ O ₄ /graphene hybrids	778 (42) @0.2 A g ⁻¹	600 @1 A g ⁻¹	0.001 – 3.0	23
Co ₃ O ₄ nanosheets-3D graphene networks	630 (50) @0.2 A g ⁻¹	130 @5 A g ⁻¹	0.05-3.0	24
Co ₃ O ₄ /Nitrogen doped graphene framework	890 (200) @0.1 A g ⁻¹	500 @5 A g ⁻¹	0.01-3.0	25
graphene wrapped TiO ₂ @Co ₃ O ₄ coaxial nanobelt arrays	437 (200) @0.1 A g ⁻¹	204@0.8 A g ⁻¹	0.005 – 3.0	26
CoO-Co ₃ O ₄ nanoribbon/RGO	994 (200) @0.1 A g ⁻¹	450 @5 A g ⁻¹	0.01-3.0	27
Co ₃ O ₄ -AP	705 (50) @0.1 A g ⁻¹	240 @5 A g ⁻¹	0.01-3.0	This work
Co ₃ O ₄ -350	1050 (50) @0.1 A g ⁻¹	808 @5 A g ⁻¹	0.01-3.0	This work

Table S4. Performance comparison of some SIB anodes based on typical Co₃O₄ structures.

materials	reversible capacity(cycles) /mA h g ⁻¹	rate capability /mA h g ⁻¹	voltage range /V, vs. Li ⁺ /Li	Ref
Co ₃ O ₄ nanocrystallites	348 (50) @0.1 A g ⁻¹	160 @4.47 A g ⁻¹	0.5-3.0	28
Shale-like Co ₃ O ₄	380 (50) @0.05 A g ⁻¹	153.8 @5 A g ⁻¹	0.005 – 2.9	29
bowl-like hollow Co ₃ O ₄ microspheres	290 (10) @0.18 A g ⁻¹	—	0.01 – 2.0	30
Co ₃ O ₄ anchored carbon nanotubes	403 (100) @0.05 A g ⁻¹	190 @3.2 A g ⁻¹	0.01-3.0	31
Co ₃ O ₄ carbon nanofiber mats	400 (700) @0.5 A g ⁻¹	401 @2 A g ⁻¹	0.01-3.0	32
Co ₃ O ₄ /MCNTs	293 (15) @0.03 A g ⁻¹	—	0.005 – 2.5	33
Mesoporous Co ₃ O ₄ sheets/3D graphene networks	523.5 (50) @0.025 A g ⁻¹	82.3 @0.5 A g ⁻¹	0.01 – 3.0	34
Monodispersed hierarchical Co ₃ O ₄ spheres/CNT	440 (30) @0.16 A g ⁻¹	184 @3.2 A g ⁻¹	0.05-3.0	35
Co ₃ O ₄ -AP	27 (50) @0.025 A g ⁻¹	17 @5 A g ⁻¹	0.01-3.0	This work
Co ₃ O ₄ -350	81 (50) @0.025 A g ⁻¹	73 @5 A g ⁻¹	0.01-3.0	This work

References

- (1) Wang, J.-Y.; Yang, N.-L.; Tang, H.-J.; Dong, Z.-H.; Jin, Q.; Yang, M.; Kisailus, D.; Zhao, H.-J.; Tang, Z.-Y.; Wang, D. Accurate Control of Multishelled Co₃O₄Hollow Microspheres as High-Performance Anode Materials in Lithium-Ion Batteries. *Angew. Chem. Int. Ed.* 2013, 52, 6417-6420.
- (2) Park, J.-S.; Cho, J.-S; Kim, J.-H.; Choi, Y.-J.; Kang, Y.-C. Electrochemical Properties of Micron-sized Co₃O₄ Hollow Powders Consisting of Size Controlled Hollow Nanospheres. *J. Alloys Compd.* 2016, 689, 554-563.
- (3) Lou, X.-W.; Deng, D.; Lee, J.-Y.; Feng, J.; Archer, L.-A.; Self-Supported Formation of Needlelike Co₃O₄ Nanotubes and Their Application as Lithium-Ion Battery Electrodes. *Adv. Mater.* 2008, 20, 258-262.
- (4) Wu, R.-B.; Qian, X.-K.; Rui, X.-H.; Liu, H.; Yadian, B.; Zhou, K.; Wei, J.; Yan, Q.-Y.; Feng, X.-Q.; Long, Y.; Wang, L.-Y.; Huang, Y.Z. Zeolitic Imidazolate Framework 67-Derived High Symmetric Porous Co₃O₄ Hollow Dodecahedra with Highly Enhanced Lithium Storage Capability. *Small* 2014, 10, 1932-1938.
- (5) Wang, Y.; Xia, H.; Lu, L.; Lin, J.-Y. Excellent Performance in Lithium-Ion Battery Anodes: Rational Synthesis of Co(CO₃)_{0.5}(OH)0.11H₂O Nanobelt Array and Its Conversion into Mesoporous and Single-Crystal Co₃O₄. *ACS Nano* 2010, 4, 1425-1432.
- (6) Sun, H.-Y.; Zhao, Y.-Y.; Mølhave, K.; Zhang, M.; Zhang, J.-D. Simultaneous Modulation of Surface Composition, Oxygen Vacancies and Assembly in Hierarchical Co₃O₄ Mesoporous Nanostructures for Lithium Storage and Electrocatalytic Oxygen Evolution. *Nanoscale* 2017, 9, 14431–14441.
- (7) Shim, H.-W.; Jin, Y.-H.; Seo, S.-D.; Lee, S.-H.; Kim, D.-W. Highly Reversible Lithium Storage in *Bacillus subtilis*-Directed Porous Co₃O₄ Nanostructures. *ACS Nano* 2011, 5, 443–449.
- (8) Tian, L.; Zou, H.-L.; Fu, J.-X.; Yang, X.-F.; Wang, Y.; Guo, H.-L.; Fu, X.-H.; Liang, C.-L.; Wu, M.-M.; Shen, P.-K.; Gao, Q.-M. Topotactic Conversion Route to Mesoporous Quasi -

- Single-Crystalline Co₃O₄ Nanobelts with Optimizable Electrochemical Performance. *Adv. Funct. Mater.* 2010, 20, 617–623.
- (9) Xiao, X.-L.; Liu, X.-F.; Zhao, H.; Chen, D.-F.; Liu, F.-Z.; Xiang, J.-H.; Hu, Z.-B.; Li, Y.-D. *Adv. Mater.* 2012, 8, 5762–5766.
- (10) Xu, J.-M.; Wu, J.-S.; Luo, L.-L.; Chen, X.-Q.; Qin, H. B.; Dravid, V.; Mi, S.-B.; Jia, C.-L. Co₃O₄ Nanocubes Homogeneously Assembled on Few-layer Graphene for High Energy Density Lithium-ion Batteries. *J. Power Sources* 2015, 274, 816–822.
- (11) Sun H.-Y.; Ahmad M.; Zhu J. Morphology-controlled Synthesis of Co₃O₄ Porous Nanostructures for the Application as Lithium-ion Battery Electrode. *Electrochim. Acta* 2013, 89, 199–205.
- (12) Huang, G.-Y.; Xu, S.M.; Lu, S.-S.; Li, L.-Y.; Sun, H.Y. Micro-/Nanostructured Co₃O₄ Anode with Enhanced Rate Capability for Lithium-Ion Batteries. *ACS Appl. Mater. Interfaces* 2014, 6, 7236–7243.
- (13) Liu, D.-Q.; Wang, X.; Wang, X.-B.; Tian, W.; Bando, Y. Golberg, D. Co₃O₄ Nanocages with Highly Exposed {110} Facets for High-performance Lithium Storage. *Sci. Rep.* 2013, 3, 2543.
- (14) Won, J.-M.; Cho, J.-S.; Kang, Y.-C. Superior Electrochemical Properties of SiO₂-doped Co₃O₄ Hollow Nanospheres Obtained Through Nanoscale Kirkendall Diffusion for Lithium-ion Batteries. *J. Alloys Compd.* 2016, 680, 366–372.
- (15) Gu, D.; Li, W.; Wang, F.; Bongard, H.; Spliethoff, B.; Schmidt, W.; Weidenthaler, C.; Xia, Y.-Y.; Zhao, D.-Y.; Schüth, F. Controllable Synthesis of Mesoporous Peapod-like Co₃O₄@Carbon Nanotube Arrays for High-Performance Lithium-Ion Batteries. *Angew. Chem. Int. Ed.* 2015, 54, 7060–7064.
- (16) Wu, F.-F.; Ma, X.-J.; Feng, J.-K.; Qian, Y.-T.; Xiong, S.-L. 3D Co₃O₄ and CoO@C Wall Arrays: Morphology Control, Formation Mechanism, and Lithium-storage Properties. *J. Mater. Chem. A* 2014, 2, 11597–11605.
- (17) Xie, Z.-Q.; Jiang, C.-M.; Xu, W.-W.; Cui, X.-D.; Reyes, C.; Martí, A.; Wang, Y. Facile Self-

- assembly Route to Co_3O_4 Nanoparticles Confined into Single-walled Carbon Nanotube Matrix for Highly Reversible Lithium Storage. *Electrochim. Acta* 2017, 235, 613–622.
- (18) Huang, G.; Zhang, F.-F.; Du, X.-C.; Qin, Y.-L.; Yin, D.-M.; Wang, L.-M. Metal Organic Frameworks Route to in Situ Insertion of Multiwalled Carbon Nanotubes in Co_3O_4 Polyhedra as Anode Materials for Lithium-Ion Batteries. *ACS Nano* 9 (2015) 1592–1599.
- (19) Dou, Y.-H.; Xu, J.-T.; Ruan, B.-Y.; Liu, Q.-N.; Pan, Y.-D.; Sun, Z.-Q.; Dou, S.-X. Atomic Layer-by-Layer Co_3O_4 /Graphene Composite for High Performance Lithium-Ion Batteries. *Adv. Energy Mater.* 2016, 6, 1501835.
- (20) Wang, Y.; Zhang, H.-J.; Lu, L.; Stubbs, L.-P.; Wong, C.-C.; Lin, J.-Y. Designed Functional Systems from Peapod-like $\text{Co}@\text{Carbon}$ to $\text{Co}_3\text{O}_4@\text{Carbon}$ Nanocomposites. *ACS Nano* 2010, 4, 4753–4761.
- (21) Yan, C.; Zhu, Y.; Li, Y.; Fang, Z.; Peng, L.; Zhou, X.; Chen, G.; Yu, G. Local Built-In Electric Field Enabled in Carbon-Doped Co_3O_4 Nanocrystals for Superior Lithium-Ion Storage. *Adv. Funct. Mater.* 2018, 28 1705951.
- (22) Wang, S.; Zhu, Y.; Xu, X.; Sunarso, J.; Shao, Z. Adsorption-based Synthesis of $\text{Co}_3\text{O}_4/\text{C}$ Composite Anode for High Performance Lithium-ion Batteries. *Energy* 2017, 125, 569–575.
- (23) Kim, H.; Seo, D.-H.; Kim, S.-W.; Kim, J.; Kang, K.; Highly Reversible $\text{Co}_3\text{O}_4/\text{graphene}$ Hybrid Anode for Lithium Rechargeable Batteries. *Carbon* 2011, 49, 326–332.
- (24) Sun, H.-Y.; Liu, Y.-G.; Yu, Y.-L.; Ahmad, M.; Nan, D.; Zhu, J. Mesoporous Co_3O_4 Nanosheets-3D Graphene Networks Hybrid Materials for High-performance Lithium Ion Batteries. *Electrochim. Acta* 2014, 118, 1–9.
- (25) Xing, X.; Liu, R.-L.; Liu, S.-Q.; Xiao, S.; Xu, Y.; Wang, C.; Wu, D.-Q. Surfactant-assisted Hydrothermal Synthesis of Cobalt Oxide/nitrogen-doped Graphene Framework for Enhanced Anodic Performance in Lithium Ion Batteries. *Electrochim. Acta* 2016, 194, 310–316.
- (26) Luo, Y.-S.; Luo, J.-S. Zhou, W.-W.; Qi, X.-Y.; Zhang, H.; Yu, D.-Y.; Li, C.-M.; Fan, H.-J.; Yu, T. Controlled Synthesis of Hierarchical Graphene-wrapped $\text{TiO}_2@\text{Co}_3\text{O}_4$ Coaxial Nanobelt

- Arrays for High-performance Lithium Storage. *J. Mater. Chem. A* 2013, 1, 273–281.
- (27) Sun, L. N.; Deng, Q.-W.; Li, Y.-L.; Mi, H.-W.; Wang, S.-H.; Deng, L.-B.; Ren, X.-Z.; Zhang, P.-X. CoO-Co₃O₄ Heterostructure Nanoribbon/RGO Sandwich-like Composites as Anode Materials for High Performance Lithium-ion Batteries. *Electrochim. Acta* 2017, 241, 252–260.
- (28) Longoni, G.; Fiore, M.; Kim, J.; Jung, Y.-M.; Kim, D.-K.; Mari, C.-M.; Ruffo, R. Co₃O₄ Negative Electrode Material for Rechargeable Sodium Ion Batteries: An Investigation of Conversion Reaction Mechanism and Morphology-performances Correlations. *J. Power Sources* 2016, 332, 42–52.
- (29) Li, H.-H.; Li, Z.-Y.; Wu, X.-L.; Zhang, L.-L.; Fan, C.-Y.; Wang, H.-F.; Li, X.-Y.; Wang, K.; Sun, H.-Z.; Zhang, J.-P. Shale-like Co₃O₄ for High Performance Lithium/sodium Ion Batteries. *J. Mater. Chem. A* 2016, 4, 8242–8248.
- (30) Wen, J.-W.; Zhang, D.-W.; Zang, Y.; Sun, X.; Cheng, B.; Ding, C.-X.; Yu, Y.; Chen, C.-H. Li and Na Storage Behavior of Bowl-like Hollow Co₃O₄ Microspheres as an Anode Material for Lithium-ion and Sodium-ion Batteries. *Electrochim. Acta* 2014, 132, 193–199.
- (31) Rahman, M.-M.; Sultana, I.; Chen, Z.; Srikanth, M.; Li, L.-H.; Dai, X.-J.; Chen, Y. Ex Situ Electrochemical Sodiation/desodiation Observation of Co₃O₄ Anchored Carbon Nanotubes: a High Performance Sodium-ion Battery Anode Produced by Pulsed Plasma in a Liquid. *Nanoscale* 2015, 7, 13088–13095.
- (32) Fu, B.; Zhou, X.; Wang, Y. Co₃O₄ Carbon Nanofiber Mats as Negative Electrodes for Sodium-ion Batteries. *Mater. Lett.* 2016, 170, 21–24.
- (33) Deng, Q.; Wang, L.; Li, L. Electrochemical Characterization of Co₃O₄/MCNTs Composite Anode Materials for Sodium-ion Batteries. *J. Mater. Sci.* 2015, 50, 4142–4148.
- (34) Liu, Y.; Cheng, Z.; Sun, H.; Arandiyan, H.; Li, J.; Ahmad, M. Mesoporous Co₃O₄ sheets/3D Graphene Networks Nanohybrids for High-performance Sodium-ion Battery Anode. *J. Power Sources* 2015, 273, 878–884.
- (35) Jian, Z.; Liu, P.; Li, F.; Chen, M.; Zhou, H. Monodispersed Hierarchical Co₃O₄ Spheres

Intertwined with Carbon Nanotubes for Use as Anode Materials in Sodium-ion Batteries. J. Mater. Chem. A 2014, 2, 13805–13809.